

# The structure of clusters in a Self-Interacting Dark Matter cosmology

Thejs Ehlert Brinckmann

Supervisor: Jesús Zavala Franco

Co-supervisor: Steen Harle Hansen

Master's thesis, submitted on August 7, 2015

Dark Cosmology Centre, Niels Bohr Institute, Juliane Maries Vej 30, 2100 Copenhagen, Denmark

## Abstract

Despite the success of the current standard model of structure formation, the Cold Dark Matter (CDM) model, the nature of dark matter remains a mystery. In particular, it is an open question whether dark matter has additional interactions other than gravity, which can impact the formation and evolution of galaxies.

Amongst these possibilities is that of Self-Interacting Dark Matter (SIDM), where dark matter can collide with itself at a significant level. SIDM shares the successes of CDM at large scales, and predicts a different dark matter distribution in the inner regions of dark matter halos. The SIDM model has the potential to solve some of the challenges faced by the CDM model, namely the core-cusp problem and the too big to fail problem.

In this thesis, I explore the SIDM model using numerical N-body simulations of a sample of 15 relaxed cluster-size halos, with the goal of analyzing their inner structure. Specifically, I quantify the difference between SIDM and CDM in the spherically averaged radial density profiles and shape of the dark matter halos. For the latter, I developed a code that computes the shape of concentric ellipsoidal shells using the eigenvalues and eigenvectors of the shape tensor. I also examine the assembly history of the halos and estimate their formation time. Unfortunately, due to constraints on computational resources I was not able to simulate a sufficient number of halos in time for the completion of this thesis and cannot draw firm conclusions. The current results, however, quantify important differences in the inner structure of clusters that in the future, with better statistics (more halos), should allow for a direct comparison with the observed shape and density of clusters of galaxies. This is a promising application with the purpose of tightening constraints on the collisionality of dark matter.

# 1 Introduction

A vast number of astronomical observations indicate that the majority of matter in the universe today is composed by “dark” particles, invisible so far to our efforts of detection. Although little is known of this dark matter, we have abundant gravitational evidence of its existence and some clues about its elusive nature. In the following I will discuss some of the main points regarding our knowledge of dark matter, that are relevant to this thesis.

## 1.1 Dark matter evidence

The first indication of the existence of “dark matter” in the universe came in 1933, when Fritz Zwicky measured the velocity dispersion of eight galaxies in the Coma galaxy cluster (Zwicky 1933 [1]). The measured velocity dispersion was much larger than expected and Zwicky concluded that the mean density of the Coma cluster must be much greater than the mean density obtained from luminous matter alone. The missing density must then come from a non-visible form of matter (dark matter). Although Zwicky overestimated the total mass to baryonic mass ratio in the Coma cluster by a large amount, modern analysis indicate that this ratio is indeed large, around 6, and thus, the cluster is held together by the invisible dark matter.

Further evidence for the existence of dark matter was provided by Babcock in 1939 [2], in the form of rotation curves for the Andromeda galaxy, which were flatter than expected, although this was not attributed to missing matter at the time. It was not until decades later that, through inferences of the circular velocity of stars and gas in many spiral galaxies, Rubin et al. (1985) [3] found out that, as a function of distance from the center of galaxies (rotation curves), the circular velocity flattens out well beyond the visible edge of the galaxy. Newtonian mechanics predicts that it should decrease as  $r^{-1}$  once the enclosed mass is constant. To preserve the Newtonian laws, one must invoke the existence of dark matter. Therefore, every galaxy is thought to be surrounded by a dark matter halo.

In addition to the velocity dispersion of galaxies in galaxy clusters and the flatness of the rotation curve of spiral galaxies mentioned above (and similarly with the velocity dispersion of stars in elliptical galaxies), which have an added value in the history of dark matter, there is a number of more recent evidences for dark matter in the universe, summarized below:

X-Ray measurements of galaxy clusters and elliptical galaxies can be used to obtain the total mass of a system via the equation for hydrostatic equilibrium, by assuming spherical symmetry and using only information obtained about the gas of the system (e.g. density and temperature). This can then be compared to the gas and stellar mass of the system and the difference is attributed to the dark matter in the system. For example, Fabricant & Gorenstein (1983) [4] measured the total mass of the giant elliptical galaxy M87 within 87 kpc using this method, obtaining  $M_{\text{tot}} = 2.1 \times 10^{13} M_{\odot}$ , within an uncertainty of 2, and  $M_{\text{gas}} = 2.1 \times 10^{11} M_{\odot}$  and since the stellar mass of such a system is of the order of the gas mass, or lower, we see that M87 is strongly dark matter dominated.

Gravitational Lensing of distant objects can be used to estimate the total matter distribution (including dark matter) of a foreground object. One of the most remarkable instances of gravitational lensing being used as proof of the existence of dark matter, is that of the two “recently” collided galaxy clusters known as the Bullet Cluster (Markevitch et al. 2002 [5]). This famous collision shows the gaseous halos (highly collisional) of the clusters lagging behind the galaxies (almost collisionless) after the collision, but gravitational lensing indicates that the majority of the mass of the systems, most of which is dark matter, is moving with the galaxies of the clusters (Clowe, Gonzalez & Markevitch 2004 [6]).

The Cosmic Microwave Background shows the structure of the universe as it was at the time of hydrogen recombination ( $\sim 380,000$  years after Big Bang). In order for that structure to evolve into the universe as we see it today a significant amount of non-baryonic matter is required. Analysis of the CMB indicates that the level of density perturbations over the background (over-density) was of the order of  $\delta\rho/\rho \sim 10^{-5}$  at the time. It is the subject of the structure formation theory to explain how the distribution of matter that we observe today, with a vast range of over-

densities, came to be from the perturbations imprinted in the CMB. Galaxies, groups and clusters have very high overdensities ( $\delta\rho/\rho \gg 1$  in galaxies), which cannot be explained without dark matter under standard gravity.

It is important to note that all the evidence we have for dark matter is gravitational and, although this evidence points to dark matter being a new type of particle, some form of modified gravity might be possible. The most popular model for departures from the law of gravity is Modified Newtonian Dynamics (MOND) (Milgrom 1983 [7]), which has some theoretical support from a relativistically covariant framework (Bekenstein 2004 [8]). However, on large scales these theories struggle and typically require some amount of dark matter (Famaey & McGaugh 2012 [9] and Angus, Famaey & Buote 2008 [10]).

## 1.2 The nature of dark matter

The nature of a potential dark matter particle remains mostly a mystery, since all we know is that it interacts gravitationally, but we do have some clues. In recent years large steps have been made in obtaining constraints on the possible mass and interactions of an as yet undiscovered particle.

**Dark matter interacts through gravity.** As mentioned previously, the only evidence we have of dark matter interactions is through its gravitational influence on visible matter.

**Dark matter has not been observed to interact with light.** The consequence of this is that dark matter must be neutral or have a very small electromagnetic coupling, otherwise we should have seen it already.

**Most of dark matter must be dissipationless** as a consequence of the last bullet point. Or, in other words, it cannot radiatively cool and collapse, as happens with baryons in galaxies. If dark matter could cool and collapse in this manner, we would not observe extended dark matter halos but disks instead. While most of the dark matter cannot radiate, it is possible that a smaller fraction (5-10%) could dissipate in such a manner, through interactions with a yet unknown “dark photon” (Fan et al 2013). This type of dark matter belongs to models that propose the existence of a rich dark matter sector, with several new particles and forces, not unlike the standard model of particle physics.

**Constraints on the possible mass of dark matter particles.** While progress has been made in recent years to constrain the possible mass of dark matter particles, a significant mass interval across many orders of magnitude is possible, from about  $10^{-33}$  to  $10^{18}$  GeV (see figure one of Gardner & Fuller (2013) [12]).

**Dark matter self-interactions are permitted within current constraints.** Observations in conjunction with the theory of structure formation in the universe rule out particles with interactions larger than the weak force (Lux coll. 2014 [13]) or very light particles (see section 1.4). While gravitation is the only interaction between dark matter particles and baryons or photons that has been detected, self interaction between dark matter particles has not been ruled out by observations (see section 1.5). This is particularly interesting, because self interacting dark matter can have a profound impact on the structure of dark matter halos. In fact, it has the potential for alleviating problems within the  $\Lambda$ CDM model, as I will discuss later in the thesis (see section 1.5).

**Dark matter requires physics beyond the Standard Model.** Although neutrinos are the obvious dark matter candidates, I will discuss later why they cannot be a major dark matter component (see section 1.4). There are no known particles that have the required properties to be the majority of dark matter.

**CDM is the most widely accepted dark matter model for structure formation.** In it, dark matter particles are cold and collisionless, the only interaction is gravity. Modern simulations show it is a very successful model that describes the evolution of the universe into the cosmic web structure we observe today and it successfully matches a variety of observations on large scales (Springel et al. 2005 [14]), and provides the cornerstone for the current theory of galaxy formation

and evolution.

### 1.3 Problems facing the $\Lambda$ CDM model

However, for all the success of the model, there is a number of significant challenges to it at sub-galactic scales, among them the core-cusp problem and the too big to fail problem:

**The core-cusp problem.** Due to the collisionless nature of CDM, the central radial density profiles of dark matter halos is predicted to be cuspy. However, several observations of dwarf galaxies and low surface brightness (LSB) galaxies indicate central density cores out to 1 kpc in radius (e.g. Kuzio de Naray et al. 2008 [15] and Walker & Peñarrubia 2011). This issue, however, remains controversial, since different groups find cusps and cores to be consistent with the data, depending on the method that is used (e.g. Breddels & Helmi 2013 [17]).

**The too big to fail problem.** Simulations of Milky Way sized systems have proven to have satellites that are too dense to be consistent with the observed kinematics of stars in Milky Way dwarf spheroidals (Boylan-Kolchin, Bullock & Kaplinghat 2011,2012 [18, 19]).

In the future, these problems could be resolved by better knowledge of the processes of galaxy formation. In particular, a better understanding of the effects of supernova feedback and tidal stripping on the formation history of dwarf and LSB galaxies (for a review see Pontzen & Governato 2014 [20]). However, it remains unclear whether significant gas removal by supernova feedback is consistent with the stellar population and star formation history of these types of galaxies.

### 1.4 Classification of dark matter in structure formation

Because of its key role in structure formation, dark matter candidates are often classified as hot dark matter (HDM), warm dark matter (WDM) or cold dark matter (CDM). These classifications are tied to the suppression, or washing out, of dark matter fluctuations in the early universe. Fluctuations below a free-streaming scale are washed out by the random thermal motions of the particles. This scale is determined by the comoving distance a particle can travel before the onset of structure formation.

**HDM.** With the exception of axions, which behave like cold dark matter, less massive ( $m_\chi \sim 30\text{eV}$ ) particles, such as neutrinos, have higher velocities and are classified as HDM. In terms of characteristic masses of the smallest structure which can form directly from the initial perturbation, the free-streaming length of the HDM particles corresponds to the mass of a large galaxy cluster. This means that for HDM, superclusters form first and fragment to form smaller structures, which is ruled out by observations (White, Frenk & Davis 1983 [21]).

**WDM.** Intermediate mass particles ( $m_\chi \sim 2\text{keV}$ ), potentially the sterile neutrino (for a review see Abazajian et al. 2012 [22]), are classified as WDM. For WDM, the free-streaming length corresponds to the mass of a dwarf dark matter halo. This means that for WDM (and CDM) structures at galactic scales and above can form directly and grow by accretion and mergers to form more massive structures in a hierarchical scenario. Structures near the free-streaming length are, however, very different in WDM compared to CDM (e.g. Lovell et al. 2014 [23]).

**CDM.** Particles with low primordial velocities, typically more massive particles ( $m_\chi \sim 100\text{GeV}$ ), which could be a supersymmetric particle or the low mass axion, are classified as CDM. Although model dependent, the canonical free-streaming length for CDM corresponds to the Earth's mass. The actual free-streaming scale for CDM is therefore irrelevant for structure formation.

### 1.5 Self-interacting dark matter

Considering the challenges facing the CDM paradigm and our limited understanding of the processes involved in galaxy formation, it is reasonable to question the central hypotheses of the CDM theory. Within the framework of the theory, it is assumed that DM particles do not interact with baryons, photons or other DM particles, except through gravity. While interaction between DM particles and ordinary matter is ruled out to very high precision by observations, as mentioned

above, constraints on the self-interacting nature of DM particles allow for significant interactions between dark matter particles.

At least one type of interaction, elastic scattering, appears to be permitted. This can take one of two different forms, velocity dependent scattering and interactions between dark matter particles using a constant cross section (Spergel and Steinhardt 2000 [24]). The latter case is the one I will investigate further in the thesis. The interaction regime of interest is a cross section per unit mass ( $\sigma/m$ ) in the range  $0.1 \text{ cm}^2 \text{ gr}^{-1}$  to  $1.0 \text{ cm}^2 \text{ gr}^{-1}$ . The reason for this interval is because it contains the region allowed by observations and the rate of interactions is sufficiently high to be of interest for galactic physics. In this range, with as little as one interaction per Hubble time, dark matter structures have markedly different properties compared to those in CDM.

The most relevant feature of self-interacting dark matter (SIDM) is that the model introduces a physical mechanism for creating dark matter cores in dwarf galaxies, by reducing the central densities of the inner halos due to the exchange of energy from the inside out due to particle collisions. Thus it can solve both the core-cusp problem and the too big to fail problem facing  $\Lambda$ CDM (see Zavala, Vogelsberger & Walker 2013 [25]).

For constant cross section SIDM, a suitably high cross section ( $\sigma/m \sim 1 \text{ cm}^2 \text{ gr}^{-1}$ ) is required to produce the desired effects while avoiding current constraints. As shown recently by Peter et al. (Peter et al. 2013 [26]) the current upper limit on constant cross section SIDM is around  $\sigma/m = 1.0 \text{ cm}^2 \text{ gr}^{-1}$ , from an analysis on the halo shapes of massive elliptical galaxies and clusters. This constraint is, however, not very precise and was done using numerical simulations in a low mass range of dark matter structures ( $10^{13} - 10^{14} M_\odot$ ). These factors motivated the present thesis.

## 1.6 Objectives of the thesis

- Learn the procedure for running numerical simulations of structure formation that follow the evolution of dark matter structure across time.
- Run high resolution simulations of cluster-size halos ( $\sim 10^{15} M_\odot$ ) in CDM and SIDM.
- Develop the tools to analyze the structure of these halos and quantify the difference between CDM and SIDM in the center of clusters.
- Discuss if those differences would make it possible to improve current constraints on the amplitude of the dark matter elastic cross section.

## 2 Simulations

Computer simulations have been of particular importance in developing the structure formation theory, serving as a tool to constrain the nature of dark matter particles and the cosmology of the Universe. The type of simulations relevant to this thesis are N-body simulations, which, in essence, are a discretization of the density field by a set of N particles whose gravitational interactions are evolved numerically through time.

### 2.1 History of simulations

An important step in the study of dark matter was the development and use of N-body simulations to study the evolution of dark matter in the universe. The history of dark matter N-body simulations begins with Press & Schechter in 1974 [27]. They used numerical simulations to test their analytical model for the evolution of cosmic structure from a density field with Gaussian initial conditions. This was closely followed in 1976 by Simon White, who simulated the formation of a Coma-like cluster (White 1976 [28]). These were pioneer studies that eventually led to the current standard model of structure formation  $\Lambda$ CDM. The following is a summary of some of the most important scientific events leading up to the currently favored cosmology,  $\Lambda$ CDM, rising to preeminence.

### 2.1.1 Scientific events leading up to $\Lambda$ CDM

**Early 1970s** Observational evidence and theoretical arguments indicated galaxies and galaxy clusters might be embedded in massive dark matter structures.

**1974 and 1976** First numerical N-body simulations of structure formation (using 1000 particles) were carried out by Press & Schechter in 1974 [27] and White in 1976 [28]. The very low number of particles and edge effects made drawing conclusions problematic.

**1978** White & Rees were the first to propose a galaxy formation theory in which gas condenses to form galaxies in the centers of dark matter structures (White & Rees 1978 [29]).

**Early 1980s** Use of Fourier calculation of long range forces increased the number of possible particles to  $N = 10^5$  (Efstatou & Eastwood 1981 [30]) and  $N = 10^6$  (Centrella & Melott 1983 [31]). Comparison with observations was still difficult because of simplistic initial conditions, uncertainty regarding the relationship between particles and galaxies and the relatively low number of particles.

**1982** First redshift survey of galaxies, the CfA redshift survey, was published (Davis et al. 1982 [32]).

**1983** Up until this time, neutrinos (HDM) had been the favored dark matter candidate. However, it became clear that the structure formation predicted by inflationary models of HDM-dominated universes were not reconcilable with the observed universe as revealed by the CfA redshift survey (White, Frenk & Davis 1983 [21]).

**1985** First CDM structure formation simulations were carried out (Davis et al. 1985 [33]). The preferred cosmology in the following years was a biased Einstein-de Sitter model called Standard Cold Dark Matter (SCDM), or in other words inflation leading to a flat universe containing no cosmological constant and galaxy placement within dark structures biased towards higher density regions.

**1998-2000** After years of contention,  $\Lambda$ CDM became the favored cosmology when supernova data ruled out the possibility of an Einstein-de Sitter universe (Riess et al. 1998 [34] and Perlmutter et al. 1999 [35]) and the CMB confirmed the universe is flat (Hanany et al. 2000 [36]).

### 2.1.2 Modern day simulations

High resolution dark matter simulations like the Millennium (Springel 2005 [14]) and Aquarius (Springel et al. 2008 [37]) projects have pushed the frontiers for numerical simulations leading to a spectacular agreement with the observed large scale structure of the Universe, and unprecedented predictions from the CDM model of the structure of our own Milky-Way halo. Simulations today are able to follow structure formation in CDM from the scales of  $\sim$ kpc within the center of dwarf scale structures to  $\sim$ Gpc tracing the large scale cosmic web (for a review see Kuhlen, Vogelsberger & Angulo 2012 [38]). The largest simulations today have trillions of particles and are run in supercomputer clusters, with allocated time of over tens of millions of CPU hours for the most expensive ones.

## 2.2 N-body simulations

As previously mentioned, an N-body simulation is a discretization of the density field in a cubic volume (box), containing  $N$  point particles with mass  $m_p$ , that is evolved in time according to the physical forces present in the problem. For cosmological simulations, the box has periodic boundary conditions and typically ranges in size from around 100 Mpc to tens of Gpc, containing millions to many billions of particles. The problem to evolve is that of the evolution of the gravitational growth of dark matter structures from an early time ( $z \sim 100$ ) until today. The initial conditions are constructed from the statistical properties of the primordial dark matter perturbations as given by the CMB.

The only interaction in a CDM N-body simulation is Newtonian gravity. Since the continuous

density field is discretized into particles, we can then get unphysical hard scatterings between particles, if they pass sufficiently close to each other. Therefore, an important parameter for N-body simulations is the gravitational softening, which plays a role on scales smaller than the softening length ( $\epsilon$ ). The value of the softening length is typically kept as small as possible (relative to the scales one wishes to resolve) and is generally given by a fraction (often around 1/20 to 1/45) of the mean interparticle separation (for a review of N-body simulations see Kuhlen, Vogelsberger & Angulo 2012 [38]).

### 2.2.1 Zoom simulations

A common zoom technique is the multimass technique. It involves selecting an area of interest in a low resolution simulation (often called the parent simulation) and re-running the simulation with higher resolution (lower mass) particles in this region. This is done while keeping the long range forces of gravity accurately represented, while computational resources are focused on the region of interest.

In practice, what is done is that the particles in the region of interest are traced back in time to their initial position in the initial conditions. These particles trace the flow of matter in the selection region through time, so this is called a Lagrangian region. In this Lagrange volume you recreate initial conditions for the simulation with higher spatial and mass resolution, while leaving the rest of the volume with a lower resolution like that of the parent simulation. Usually a number of intermediate resolution buffer regions are added around the high resolution region.

The advantage of these zoom simulations, is that you can run simulations with a large enough box to simulate a cosmological volume but with sufficient resolution to study galaxy or cluster sized structures, while minimizing computational time (for an introduction to zoom simulations see Oñorbe et al. 2014 [39]).

### 2.2.2 SIDM in simulations

The simulations used for this thesis were run with the N-body code Gadget 3 (last described in Springel et al. 2005 [14]), with an extra module for computing interactions between the particles (Vogelsberger, Zavala & Loeb 2012 [40]). This module computes the elastic scatterings between pairs of particles via an N-body Monte Carlo method that implements the physical consequences of the interactions in a statistical, probabilistic sense, with the interaction rate given by (Rocha et al. 2013 [41])

$$\Gamma_{\text{loc}} = \rho_{\text{loc}} \frac{\sigma}{m_\chi} v_{\text{rms,loc}} \quad (1)$$

where  $\rho_{\text{loc}}$  is the local density,  $\sigma/m_\chi$  is the cross section per unit mass and  $v_{\text{rms,loc}}$  is the root mean square of the local velocity. If a pair is selected for collision, this gives rise to an elastic scattering and the new velocities of the particles are then given by:

$$\mathbf{v}_i = \mathbf{v}_{\text{cm}} + (\mathbf{v}_{ij}/2)\hat{e} \quad (2)$$

$$\mathbf{v}_j = \mathbf{v}_{\text{cm}} - (\mathbf{v}_{ij}/2)\hat{e} \quad (3)$$

Where  $\mathbf{v}_{\text{cm}}$  is the center of mass velocity of the two particles,  $\mathbf{v}_{ij}$  is the relative velocity between the particles and  $\hat{e}$  is a unit vector randomly selected from the unit sphere.

## 2.3 What are the most important statistics I will analyze?

Dark matter halos are the fundamental non-linear building blocks of the Universe. Structures from the smallest dwarf galaxies to the largest galaxy clusters appear to exist in large enveloping dark matter halos. A halo is a gravitationally self-bound dark matter structure that has separated from the global expansion of the Universe. Although dark matter halos are triaxial with important non-spherical features, it is a common practice to analyze their structure through spherically averaged radial profiles from their center.

The important statistics that will be analyzed in this thesis are the density profile and the halo

shapes, which together give a measure of the halo structure. In addition to the density as a function of radius, I will also be examining the ratio between the minor and major axes and the intermediate and major axes as a function of radius. I will be looking at the difference between CDM and SIDM at different radii, in order to obtain a measure of the effect of increasing the scattering cross section.

We are interested in studying dynamically relaxed systems, which could potentially be compared with observed clusters with no obvious sign of recent mergers. Therefore, I adopt the criteria described in (Ludlow et al. 2012 [42]) to select a subsample of relaxed haloes from our parent simulation (see section 2.4 below):

- (i) The subhalo mass fraction must be below 10% ( $f_{\text{sub}} = M_{\text{sub}}/M_{200} < 0.1$ ). Otherwise, very massive subhalos might perturb the halo significantly.
- (ii) The distance between the center of mass of the halo and its potential minimum, in units of the virial mass, must be less than 0.07 ( $d_{\text{off}} = |r_{\text{pot}} - r_{CM}| < 0.07$ ). A larger difference indicates a substantial merger is in progress.
- (iii) The virial ratio of total kinetic to potential energies must be less than 1.35 ( $2T/|U| < 1.35$ ), this is the criterion for virialization, dynamical equilibrium.

## 2.4 Description of the simulations used in the Thesis

The parent simulation I used is a 1 Gpc<sup>3</sup> box, containing 512<sup>3</sup> dark matter simulation particles. The zoom simulations used for the analysis have a resolution of 4096<sup>3</sup> particles for the high resolution region, which means if the entire box was this resolution, it would contain 4096<sup>3</sup> particles. This high resolution region is surrounded by regions of intermediate resolution and finally a low resolution volume with an effective resolution of 256<sup>3</sup> particles. The mean interparticle separation in the initial conditions for the high resolution region is  $dx = 244.141 \text{ kpc h}^{-1}$ . For the softening I used  $\epsilon = dx/45$ , so the softening used for the high resolution region is  $\epsilon = 5.42534 \text{ kpc h}^{-1}$ . We run simulations in CDM and in SIDM with two values for the scattering cross section:  $\sigma/m_\chi = 1 \text{ cm}^2 \text{ gr}^{-1}$  (SIDM1) and  $\sigma/m_\chi = 0.1 \text{ cm}^2 \text{ gr}^{-1}$  (SIDM 0.1).

We can calculate a radius that gives an indication of the lowest radius at which we can trust the density and halo shapes profiles (Power et al. 2003 [43]) (I will return to this in section 2.6), the so called power radius. This is done by finding the minimum radius that satisfies (the following is based on (Springel et al. 2008 [44])):

$$\frac{\sqrt{200}}{8} \frac{N(r)}{\ln(N(r))} \left[ \frac{\bar{\rho}(r)}{\rho_{\text{crit}}} \right]^{-1/2} \geq 1 \quad (4)$$

Here  $N(r)$  is the number of particles within a radius  $r$ ,  $\bar{\rho}(r)$  is the mean density within  $r$  and  $\rho_{\text{crit}} = 3H^2/(8\pi G)$  is the critical density of the universe today. We have that the mean density within  $r$  is

$$\bar{\rho}(r) = \frac{N(r)m_p}{r^3} \quad (5)$$

where  $m_p$  is the particle mass. For an NFW profile (Navarro, Frenk & White 1997 [45]), which is a good description of CDM halos, the number of particles within  $r$  is given by

$$N(r) = \frac{M_{\text{NFW}}(r)}{m_p} \quad (6)$$

where  $M_{\text{NFW}}(r)$  is the mass within  $r$ :

$$M_{\text{NFW}}(r) = 4\pi\rho_s r_s^3 \left[ \ln\left(\frac{r_s + r}{r_s}\right) - \frac{r}{r_s + r} \right] \quad (7)$$

where  $r_s$  and  $\rho_s$  are a characteristic radius and density, respectively. For the scale radius we can use  $r_s = R_{200}/c$ , where  $c$  is the concentration, while  $\rho_s$  can be obtained from

$$\delta_c = \frac{\rho_s}{\rho_{\text{crit}}} = 7.213\delta_V \quad (8)$$

$\delta_V$  is

$$\delta_V = \frac{\bar{\rho}(r_{\max})}{\rho_{\text{crit}}} = 2 \left( \frac{V_{\max}}{H_0 r_{\max}} \right)^2 \quad (9)$$

where we have both  $V_{\max}$ , which is the maximum circular velocity, and  $r_{\max}$ , the radius where  $V_{\max}$  is attained, from our simulated halos using the halo catalogue information extracted with the code SUBFIND (Springel et al. 2001). We can use  $\delta_c$  to find the concentration via

$$\delta_c = \frac{200}{3} \frac{c^3}{\ln(1+c) - c/(1+c)} \quad (10)$$

giving us all we need to calculate the power radius, which we refer to as the trust radius. This is approximately  $r_{\text{trust}} \approx 40 \text{ kpc h}^{-1}$  at the resolution level we use for most of our results.

To obtain the zoom simulations I did the following:

1. Pick “relaxed” halos in the parent simulation.
2. Use my own code to select the Lagrangian region containing the halo particles and surrounding area at  $z=0$  in the parent simulation.
3. Traceback the particles to the initial redshift  $z=50$  using my own code, by matching the particle ID numbers between redshifts.
4. Compute initial conditions for the zoom simulation using MUSIC (Hahn & Abel 2011 [46]), specifying the ellipsoidal (or cuboid) region containing the particles at  $z=50$  as the high resolution region.
5. Run zoom simulations of each individual halo based on the initial conditions generated by MUSIC, switching the particle interaction module for the SIDM simulations.

Of the  $\sim 40$  relaxed halos found in the box with masses  $M_{200} > 6.5 \times 10^{14} M_\odot h^{-1}$ , I have so far simulated 15. These will be the ones analyzed in this thesis.

For the 15 halos, the radius within which the average density of each halo is 200 times the critical density of the universe covers a range of  $R_{200} \approx 1500 - 2000 \text{ kpc}$  and we have that the mass within  $R_{200}$  covers a range of  $M_{200} \approx 0.8 - 1.9 \times 10^{15} M_\odot$ , with a high resolution particle mass of  $m_p = 1.271 \times 10^9 M_\odot$ .

Figure 1 shows the distributions in  $M_{200}$  and  $R_{200}$  for the 15 halos simulated for this thesis. Except for the most massive cluster, the sample has a narrow distribution centered around  $M_{200} \sim 0.9 \times 10^{15} M_\odot h^{-1}$  and  $R_{200} \sim 1550 \text{ kpc h}^{-1}$

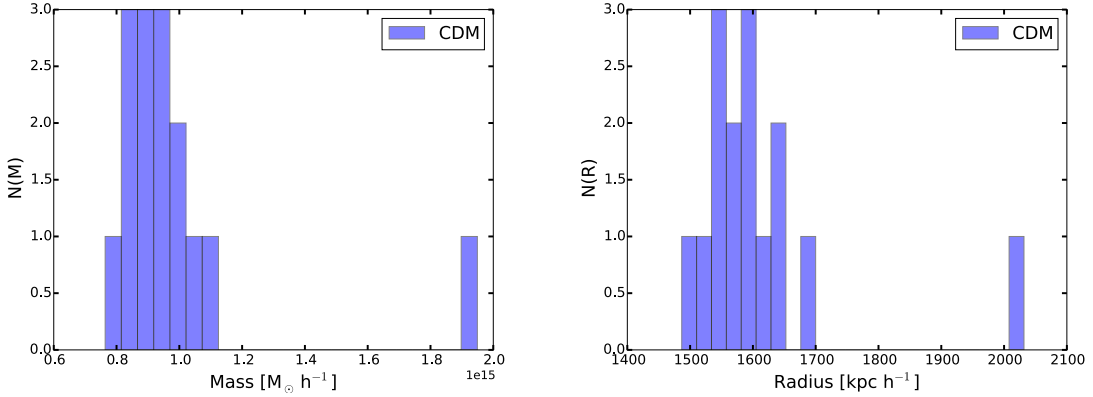


Figure 1: *The distribution of virial masses and radii for the 15 simulated CDM halos used in this thesis.* **Left:** Number of halos vs virial mass. Except for one outlier near  $1.9 M_\odot h^{-1}$ , we have a heavily peaked distribution around  $0.9 M_\odot h^{-1}$ . **Right:** Number of halos vs virial radius. We see a peaked distribution around  $1550 kpc h^{-1}$ , with the same halo as before showing up as an outlier at near  $2000 kpc h^{-1}$ . For the SIDM 1 and SIDM 0.1 halos (not shown) the distributions are virtually the same, because SIDM does not alter the virial mass or radius of a halo in any significant way.

## 2.5 Analysis tools

**Density profiles.** In order to obtain the density profile of the simulated halos, the center of the potential is taken as the center of the halo. From here the density is calculated in concentric radial shells by summing up the mass of the particles and dividing by the volume.

**Halo shapes code.** For the purpose of determining the halo shapes of the simulated dark matter halos, I created a halo shapes code based on the methods described in Zemp et al. 2011 [47]. The method in question uses the eigenvectors and eigenvalues of the shape tensor of the distribution of particles, in order to determine the orientation and magnitude of the principle axes of the halo. In essence the code divides the halo into a number of ellipsoidal shells and for each shell iteratively finds the shape of the shell by calculating the eigenvectors and eigenvalues of the momentum shape tensor of the shell particles, until convergence of the eigenvalues is obtained. It typically takes between 20 to 40 iterations for convergence to be obtained, but a low number of particles or a very spherical system can cause the code to struggle and not converge in a reasonable time frame. For each iteration, the code deforms the volume of the ellipsoidal shell according to the previous result, while keeping the size of the major axis constant. This means a new set of particles is selected for each iteration, until convergence is obtained and the set of particles is roughly constant.

Central to the halo shapes code is the shape tensor. From Zemp et al. 2011 [47] we have the definition of the shape tensor as

$$\mathbf{S} \equiv \frac{\mathbf{M}}{M_{\text{tot}}} = \frac{\int_V \rho(\mathbf{r}) \mathbf{r} \mathbf{r}^T dV}{\int_V \rho(\mathbf{r}) dV} \quad (11)$$

where  $\rho$  is the density and  $\mathbf{r}$  is the radius.  $M_{\text{tot}} = \int_V \rho(\mathbf{r}) dV$  is the total mass of the system and  $\mathbf{M}$  describes the matter distribution of the system and is related to the moment of inertial tensor via

$$\mathbf{I} = \text{tr}(\mathbf{M}) \mathbf{1} - \mathbf{M} \quad (12)$$

where  $\mathbf{1}$  is an identity tensor. Discretizing the individual elements of the shape tensor we have:

$$S_{ij} = \frac{\sum_k m_k (\mathbf{r}_k)_i (\mathbf{r}_k)_j}{\sum_k m_k} \quad (13)$$

Where  $m_k$  is the mass of the k'th particle (in our case all the particles in the high resolution region have the same mass) and  $(\mathbf{r}_k)_i$  is the i'th component of the position vector of the k'th particle. Likewise with  $(\mathbf{r}_k)_j$  for the j'th component. In our case the mass cancels and we are left with:

$$S_{ij} = \sum_k (\mathbf{r}_k)_i (\mathbf{r}_k)_j \quad (14)$$

Which is the fundamental equation of the halo shapes code.

I implemented additional options in halo shapes code for variable particle mass and a number of different halo shapes methods. Depending on which flag is set, the code can either keep the major axis of the shell fixed (as described above) or the volume of the shell constant. There is also the option to calculate the halo shapes based on the entire enclosed mass (as opposed to a shell) or weight the contribution of each particle to the shape tensor by the elliptical radius  $r_{\text{ell}} = \sqrt{x_{\text{ell}}^2 + \frac{y_{\text{ell}}^2}{(b/a)^2} + \frac{z_{\text{ell}}^2}{(c/a)^2}}$ , where  $x_{\text{ell}}$ ,  $y_{\text{ell}}$  and  $z_{\text{ell}}$  is the distance along the principal axes of the ellipsoid and  $a$ ,  $b$ ,  $c$  are the major, intermediate and minor axes, respectively.

### 2.5.1 Test of halo shapes code

I tested my halo shapes code with a number of halos with known properties and the code successfully and consistently obtained halo shapes estimates very close to the true halo shape. The halos were generated using Marcel Zemp's HALOGEN code (Zemp et al. 2008 [48]). I used halos with a number of different shapes, including halos that were very spherical, prolate or oblate and halos rapidly increasing or declining in ellipticity as a function of radius. Additionally, I used different density profiles given by

$$\rho(r) = \rho_s / [(r/r_s)^\gamma] [1 + (r/r_s)^\alpha]^{[(\beta - \gamma)/\alpha]} \quad (15)$$

where  $\rho_s$  and  $r_s$  is scale density and radius, respectively. I set  $\alpha = 1$ ,  $\beta = 3$  and  $\gamma = 1$  to obtain an NFW profile with cuspy central densities and  $\gamma = 0$  to obtain a profile with cored central densities.

I tested the different methods of the halo shapes code outlined above (see section 2.5), the most accurate ones are shown in Figure 2. We see that the method keeping the size of the major axis fixed is the most successful method, and this is the method I will be using in the remainder of the thesis.

The code has a tendency to slightly overestimate, by about 8-9% for well converged bins, the axis ratios for halos increasing in ellipticity with radius (see left column of Figures 3 and 4) and slightly underestimate by a similar amount, the axis ratios for halos with decreasing ellipticity (see right column of Figures 3 and 4). Additionally, I find that the code struggles to estimate halo shape of very spherical systems, and results for such systems cannot be trusted to more than approximately 10%.

However, the most severe constraint on the accuracy of the code is particle number within a given ellipsoidal shape, as is seen by comparing the inner structure (< 100 kpc) of the halos in Figures 3 and 4. The former has a cuspy density profile (resembling CDM halos) and thus more particles in the inner region, whereas the latter has a cored density profile (resembling SIDM halos) and therefore fewer particles in the center. Obtaining convergence for shells with much fewer than  $\mathcal{O}(10^4)$  particles is often problematic and results are less accurate (or simply fail to converge). This is seen for the inner bins in Figure 4, where the results are overestimated or underestimated by as much as about 20%. This is something to keep in mind if we attempt to analyze SIDM (cored) halos close to center. For the analysis in this thesis I used a minimum of  $\mathcal{O}(10^3)$  particles (1500 for the initial spherical shell).

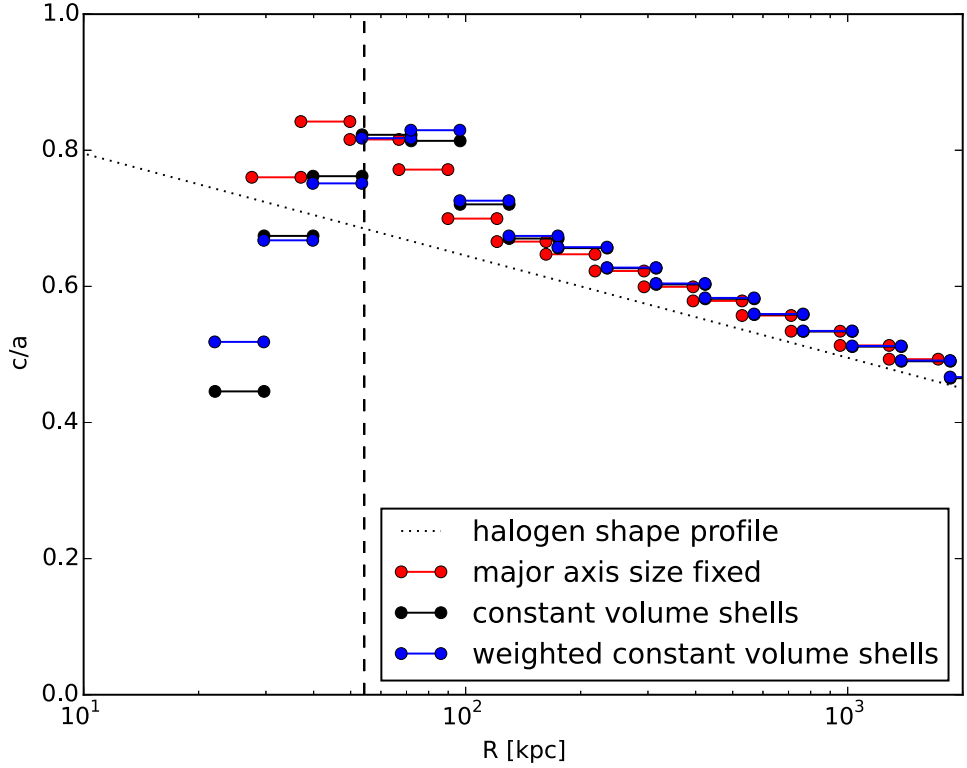


Figure 2: Comparison of the most accurate halo shapes methods of my code, using known halo shape profiles created using HALOGEN (Zemp et al. 2008 [48]). The figure shows the ratio of the minor ( $c$ ) to major axis ( $a$ ) vs radius, with the analytical halo shape profile used in HALOGEN indicated by a black dotted line ( $\gamma = 0$  was used for the density profile, see eq 15). The vertical dashed line marks ten times the softening for this simulation. Above this line the different methods are reliable. We see that the method with the size of the major axis fixed (red bins) is somewhat more accurate than the methods keeping the volume of the shells constant (black and blue bins). For the rest of the thesis we will be using only the fixed major axis method.

$$\gamma = 1$$

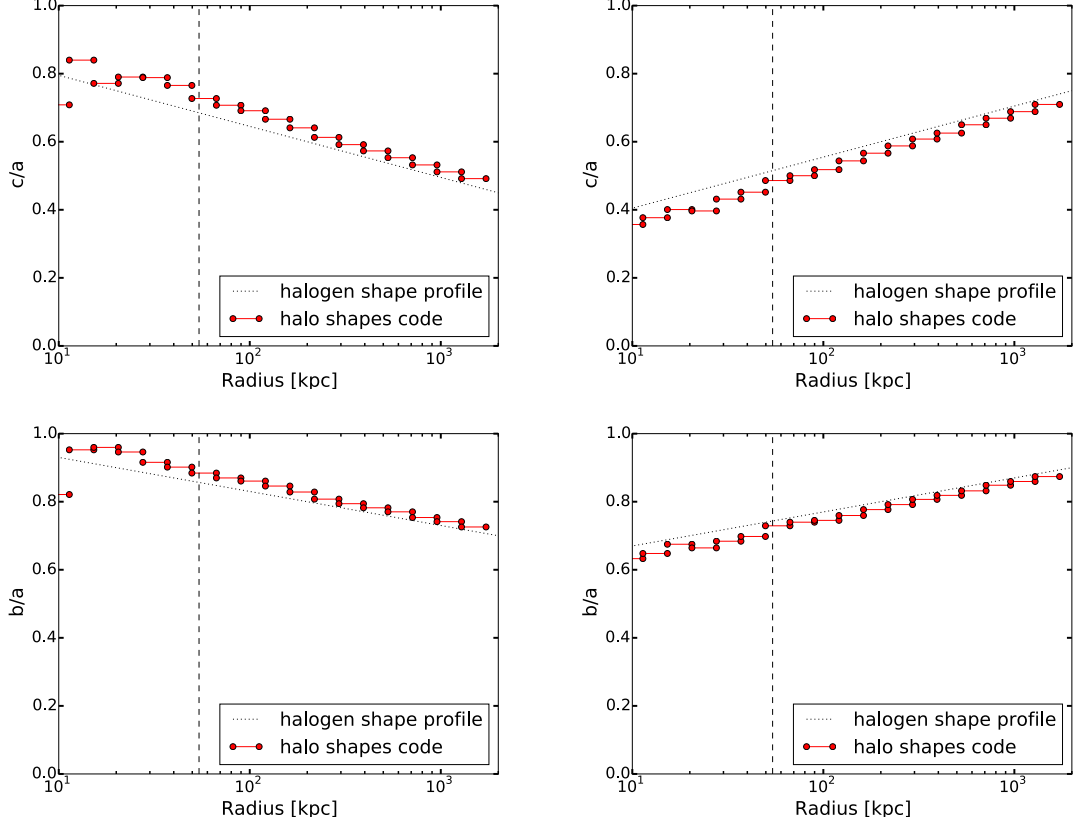


Figure 3: The halo shapes for two distinct halos with cuspy central densities ( $\gamma = 1$ , see equation 15). The analytical halo shape profiles are shown by black dotted lines. The black dashed line indicates ten times the softening, which is a measure of a radius above which we can trust the halo shapes results, and the red bins show the result of my halo shapes code. **Top row:** Ratio of the size of the minor to major axis vs radius. **Bottom row:** Likewise for the intermediate and major axes. **Left column:** We clearly see the halo shapes code slightly overestimates, by  $\sim 8\%$ , the halo shape profile of halos declining in sphericity with radius. **Right column:** Similarly, for halos increasing in sphericity with radius the code underestimates, again by about  $\sim 8\%$ , the halo shape profile.

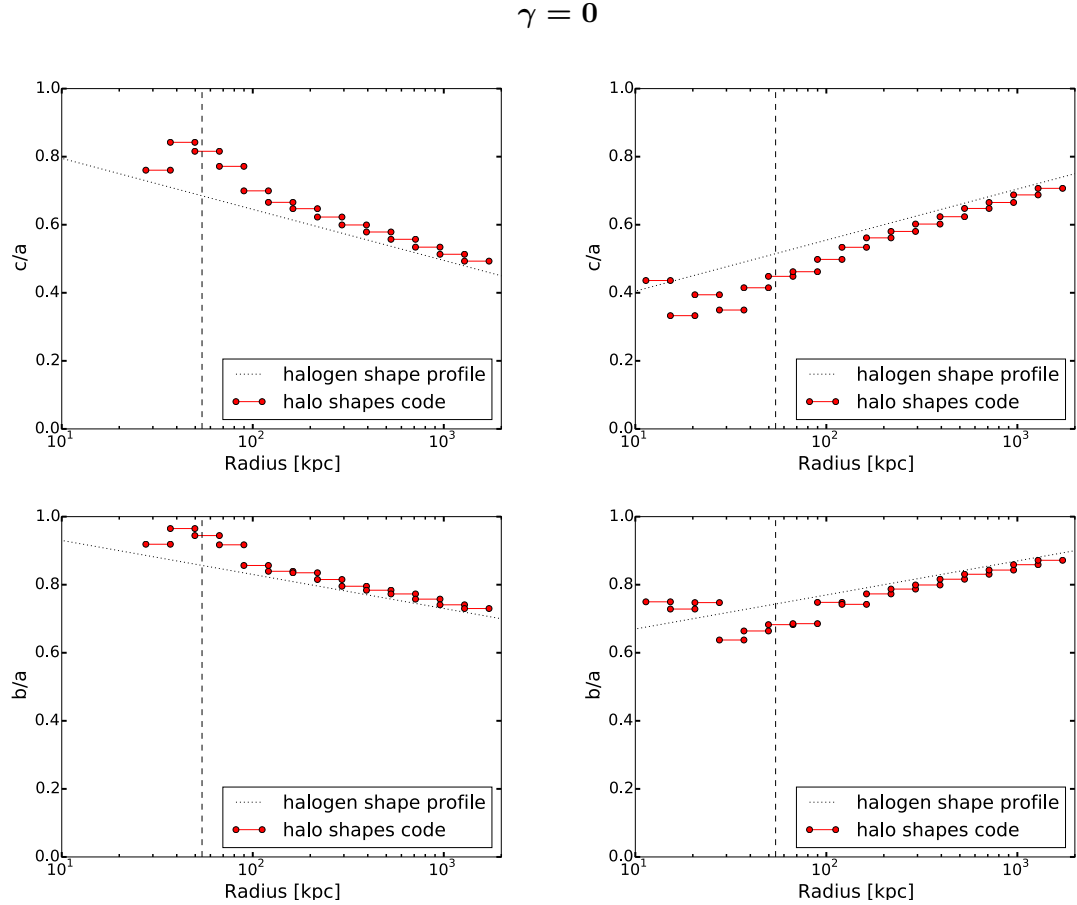


Figure 4: Similarly shows the halo shapes, but for two  $\gamma = 0$  halos (see equation 15) with cored central densities. The results from the halo shapes code is shown as red bins and the analytical halo shape profiles are denoted by black dotted lines. A measure of the radius beyond which we can trust the results is indicated by ten times the softening as a black dashed line. **Top row:** Ratio of the size of the minor to major axis vs radius. **Bottom row:** Likewise for the intermediate and major axes. **Left column:** We see that for halos with increasing ellipticity with radius the halo shapes are again overestimated (see Figure 3), by less than  $\sim 10\%$ , for the well converged bins. However, we see that due to the low number of particles at lower radii (because of the cored central densities of the halos), the halo shapes code struggles to converge and overestimates the halo shape by as much as  $\sim 20\%$ . **Right column:** Again the code underestimates, by less than  $\sim 10\%$  the halo shape for halos decreasing in ellipticity with radius, but struggles close to the center, underestimating the halo shape by almost  $\sim 20\%$ .

## 2.6 Convergence

I did a number of convergence tests for one of the halos (the most massive one) in order to eliminate numerical artefacts. I do convergence tests across resolution, the size and type of the Lagrangian region. The properties of interest in these tests are the density profile and the halo shapes. I also checked the level of contamination, i.e. the number of lower resolution particles in the high resolution region, which I found to be non-existent to negligible.

In order to test which type of Lagrangian region was optimal (cuboid or ellipsoidal around a halo of interest), I ran simulations with resolutions corresponding to  $2048^3$  and  $4096^3$  particles for the high resolution region. I did not find any significant difference between ellipsoidal and cuboid Lagrangian volumes, so I used an ellipsoidal Lagrangian region for the rest of the simulations, in order to save computational time, due to its reduced volume (see Figure 5, the differences are at

the percent level for  $r > r_{\text{trust}}$ ).

For testing the size of the ellipsoidal Lagrangian region, I used a fixed resolution corresponding to  $4096^3$  particles for the high resolution region and I varied the size of the ellipsoid to include 12, 13, 15 and 17 times the virial radius of the halo ( $R_v$ ). I found some numerical artefacts using a Lagrangian region size of 12  $R_v$ , whereas 13, 15 and 17  $R_v$  did not display significant differences. In order to save computational time, I used a Lagrangian region size of 13  $R_v$  for the rest of the simulations.

For the resolution tests I used three different levels of resolution for the zoom region corresponding to  $2048^3$ ,  $4096^3$  and  $8192^3$  particles (see Figure 6). This figure gives a quick impression of the differences between resolution levels and it also shows the main features that distinguish SIDM halos from CDM ones: A central spherical core instead of a cuspy triaxial central region. As anticipated, a resolution corresponding to  $2048^3$  particles does not resolve the inner halo structure to the degree necessary to fulfill our objectives, while a resolution corresponding to  $4096^3$  particles is reasonably well converged (to  $3\epsilon$  for the density profile and  $r_{\text{trust}}$  for the halo shapes) with respect to that of the highest resolution I ran ( $8192^3$ ) (see Figure 7). Although using a higher resolution corresponding to  $8192^3$  particles would be able to provide a clearer picture of the inner halo structure of the simulated halos, the computational time to run a suitable number of simulations was prohibitive relative to the scope of the project (taking 5-10 times longer per simulation).

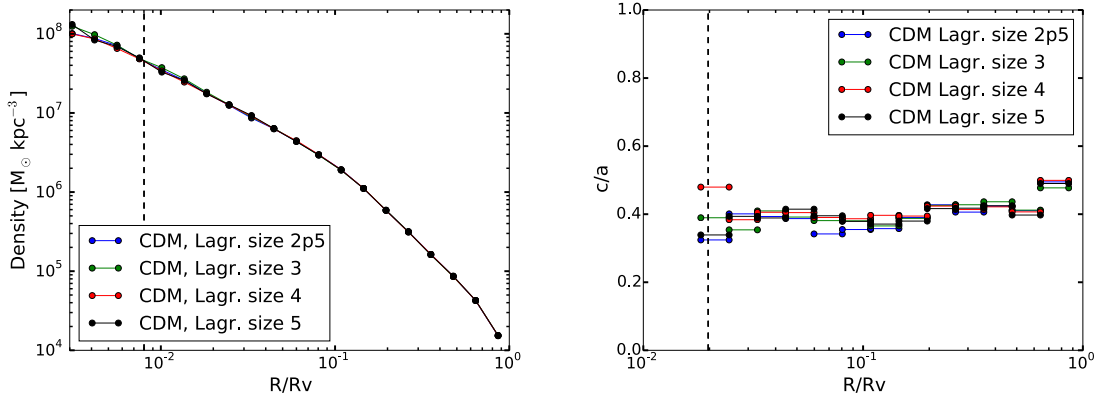


Figure 5: *Convergence plots for the Lagrangian region size. In the legend size 2p5, 3, 4 and 5 denote sizes of 12 (blue), 13 (green), 15 (red), 17 (black) times the virial radius respectively. The vertical dashed lines indicate the trust radius. **Left:** Density vs radius scaled by the virial radius. The figure shows the density profile of zoom simulations of the most massive halo. We see the Lagrangian region size has virtually no effect on the profile. **Right:** Ratio of minor to major axis for the same four CDM simulations of the most massive halo. We see that beyond the trust radius they are all fairly close within a few percent, except for the 12  $R_v$  simulation, which shows some difference.*

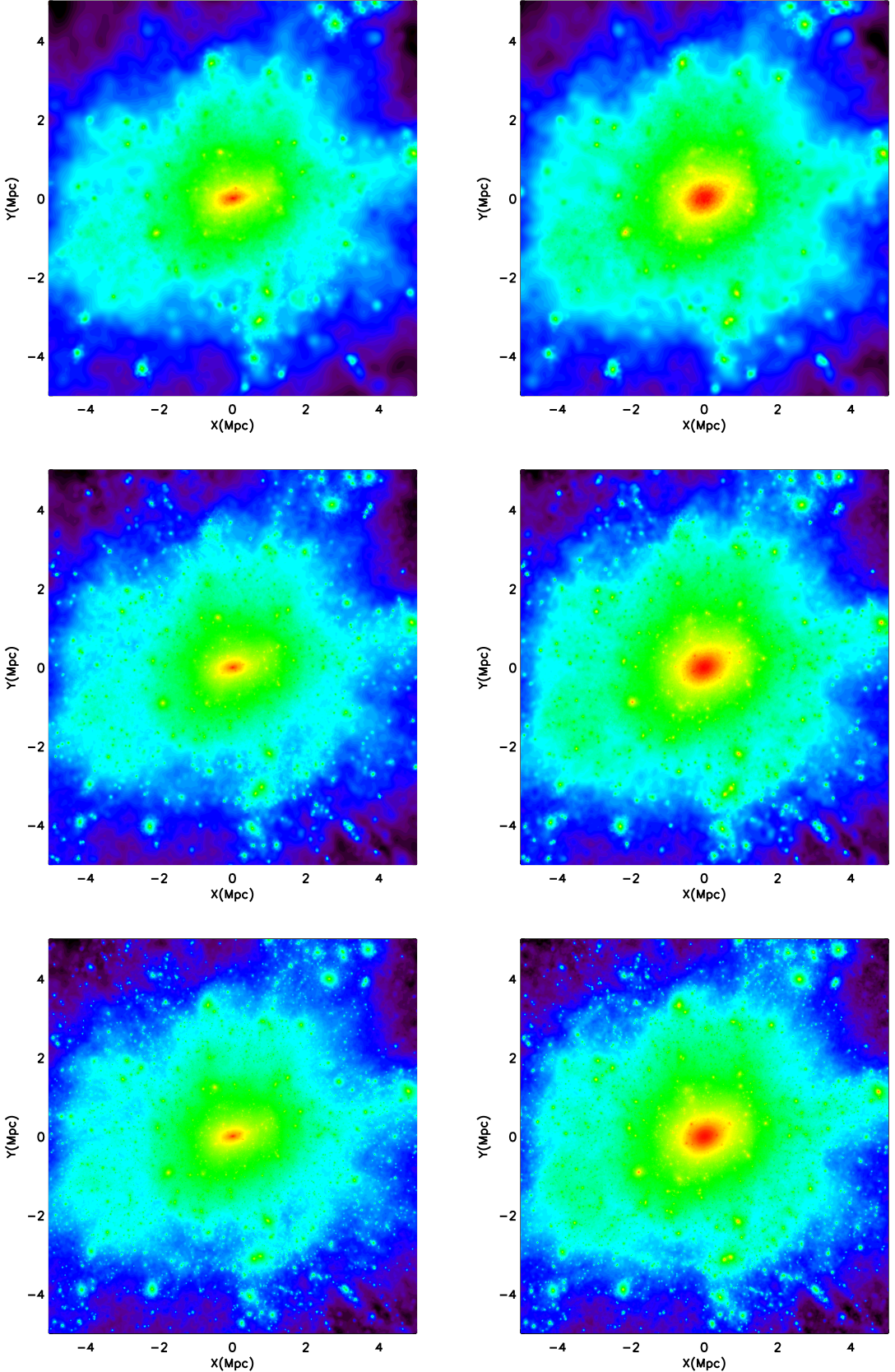


Figure 6: Visualization plots showing the projected density for  $y$  vs  $x$ . **Left column:** CDM simulations of the most massive halo at resolution levels  $2048^3$ ,  $4096^3$  and  $8192^3$ , from top to bottom. We see the effect of resolution in resolving substructure and we can see the highly triaxial cuspy central density. **Right column:** SIDM 1 simulations of the same halo at the same resolution levels. We see the cored central density typical of SIDM, with a more spherical central density.

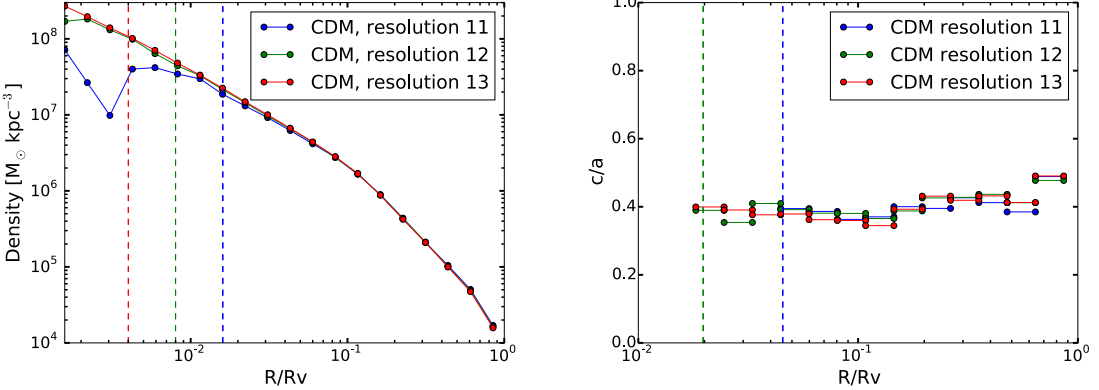


Figure 7: *Convergence plots for the resolution. The most massive halo was simulated in a CDM cosmology at three different resolution levels:  $2048^3$  (denoted 11, in blue),  $4096^3$  (denoted 12, in green) and  $8192^3$  (denoted 13, in red).* **Left:** The density vs the radius scaled by the virial radius. The vertical dashed lines indicate the trust radius (3 times the softening for the density profiles) for each of the three resolution levels (low in blue, intermediate in green and high in red). We see that the low and intermediate resolution density profiles are well converged beyond the trust radius, when compared to the high resolution one. **Right:** The ratio of minor to major axis vs radius scaled by the virial radius. The vertical dashed lines indicate the trust radius for each resolution level (low in blue, intermediate in green), please note the red (high resolution) would be to the left, outside the figure. We see that outside the trust radius for a given resolution, the halo shapes are converged, to within a few percent, for the low and intermediate resolutions, when compared to the high resolution simulation.

### 3 Results

#### 3.1 Density profiles

I created combined density profile distributions for each of the three types of simulations, CDM, SIDM1 and SIDM0.1, for all our simulated halos (i.e. stacking all 15 halos). This is shown in Figure 8, where the central lines are the medians of the distributions and the shades of the regions indicate the one sigma regions of each distribution.

Figure 8 shows important differences between CDM and SIDM above the minimum radius we can trust for all our halos ( $R/R_v \sim 10^{-2}$ , dashed line). The SIDM 1 halos have a clear core with a size of  $R_{\text{core}} \sim 6 \times 10^{-2}$  with a central density of  $\sim 6 \times 10^6 M_{\odot} \text{ kpc}^{-3}$ , a factor of  $\sim 7$  smaller than CDM at  $R/R_v \sim 10^{-2}$ . The SIDM 0.1 case is much closer to CDM, but our resolution is enough to clearly separate the halo distributions (at the  $1\sigma$  level) at  $R/R_v \sim 10^{-2}$ . This is a radius well within the inner region of the clusters ( $\sim 15$  kpc), where the effects of the luminous matter in the dark matter distribution are quite important. This makes the level of  $0.1 \text{ cm}^2 \text{ gr}^{-1}$  a difficult target to reach using DM-only simulations. The situation near a value of  $1.0 \text{ cm}^2 \text{ gr}^{-1}$  is very different, here there is a clear separation already at  $\sim 100$  kpc, far from the influence of baryons. Our simulations can then be used with confidence to constrain SIDM at this level.

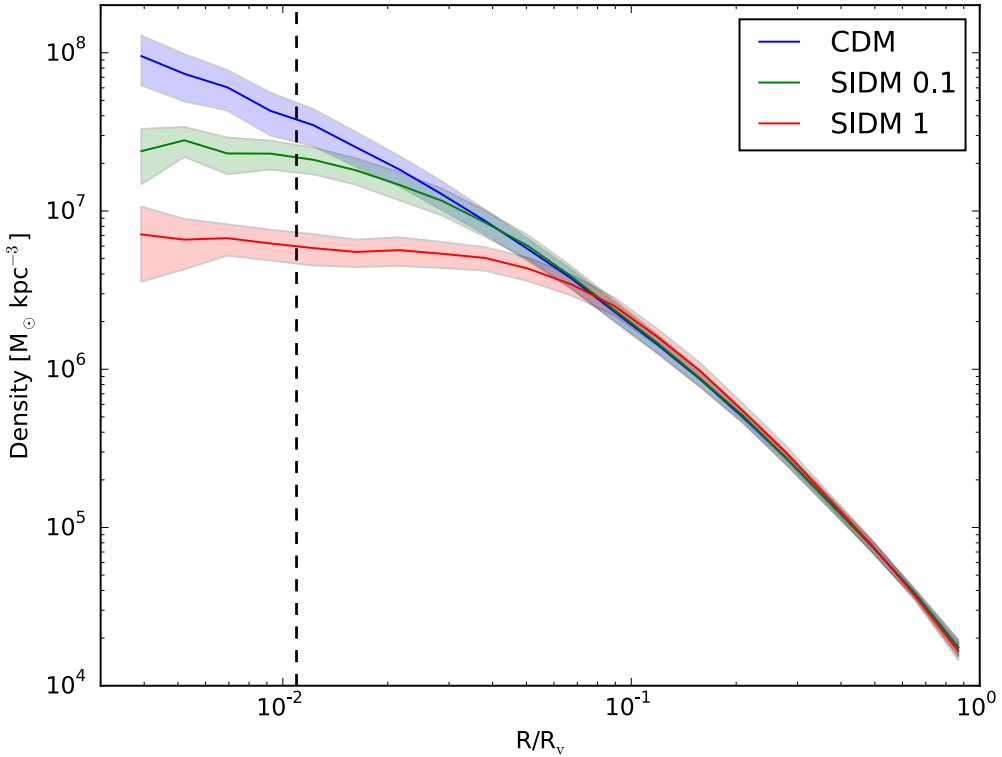


Figure 8: *Density vs radius scaled by the virial radius ( $R/R_v$ )*. Shown is the density profile of a distribution of 15 cluster-size halos, where the radius of each halo is scaled by its virial radius, for each of the three different types of simulation (CDM in blue, SIDM 0.1 in green and SIDM 1 in red). The median of each distribution is shown as a solid line and the shaded region indicates the standard deviation of the distribution. The dashed line indicates three times the softening ( $\epsilon$ ) of the simulations scaled by the virial radius of the smallest halo, which is the radius to which we can reliably trust the stacked density profiles. As expected, we clearly see cored central densities for the SIDM 1 halos and also a clear tendency at  $R > 3\epsilon$  towards less cuspy central densities for the SIDM 0.1 halos.

### 3.2 Halo shapes

I created combined (stacked) halo shapes profile distributions in the form of the principal axis ratios  $c/a$  and  $b/a$ , for all our simulated halos. This is shown in Figure 9, where the central lines indicate the medians of the distributions and the shaded regions indicate the one sigma regions of the distribution.

Figures 9 and 10 show that already with the sample of halos I have simulated, we can use the halo shapes to distinguish CDM from SIDM 1 for massive clusters within most of the radial range; except very close to the virial radius. Although my halo shapes code has some problems around the trust radius, we can clearly see that between  $5 \times 10^{-2} \lesssim R/R_v \lesssim 3 \times 10^{-1}$  the SIDM 1 and CDM distributions do not overlap at the  $\sim 1\sigma$  level.

Although the code has some biases (see section 2.6), they are expected to be of similar magnitude for both CDM and SIDM 1, therefore we are optimistic that our simulations can be used to reliably test the amplitude of a possible dark matter cross section  $1.0 \text{ cm}^2 \text{ gr}^{-1}$ . We notice that at the  $1\sigma$  level, the halo shapes separate at larger radii than the density profiles, making this method potentially more free of baryonic effects.

The SIDM 0.1 case is unfortunately too close to CDM even at the lowest radii we can trust. A more detailed analysis of the actual distributions of  $c/a$  ( $b/a$ ) at a small fixed radius might indicate to which extent we can separate both cases.

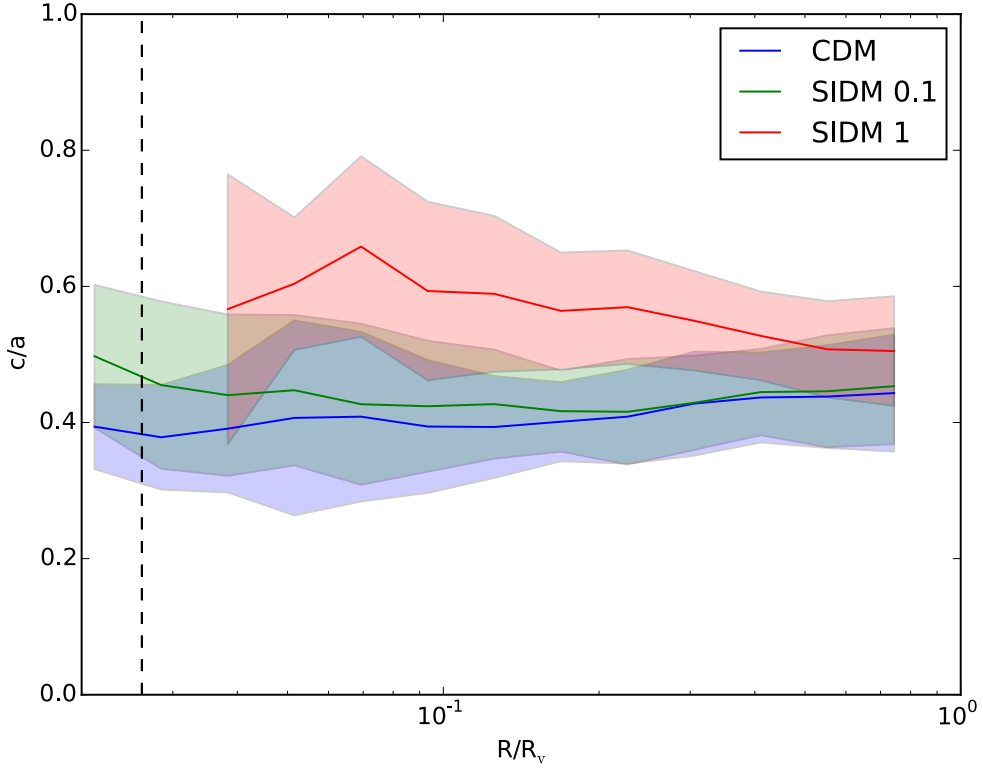


Figure 9: *Ratio of the minor to major axis ( $c/a$ ) vs radius scaled by the virial radius of each halo ( $R/R_v$ ). The figure shows the combined distribution of 15 halos of each of the three different simulation types (CDM in blue, SIDM 0.1 in green and SIDM 1 in red). The central line for each distribution is given by the median of the distribution and the standard deviation is indicated by the shaded region. The trust radius (see section 2.4) is indicated as a vertical dashed line. We see that for the SIDM 1 distribution (red), the trust radius is too optimistic. This is due to the cored central densities of these halos (see Figure 8), resulting in too few particles for the halo shapes code to reliably converge. Nevertheless, the differences between SIDM1 and CDM are clear at all radii. We see a hint of divergence between the CDM (blue) and SIDM 0.1 (green) distributions at  $R/R_v < 0.1$ , but unfortunately the statistics are too poor to draw any firm conclusions. With an increased number of halos it should be possible to quantify this divergence.*

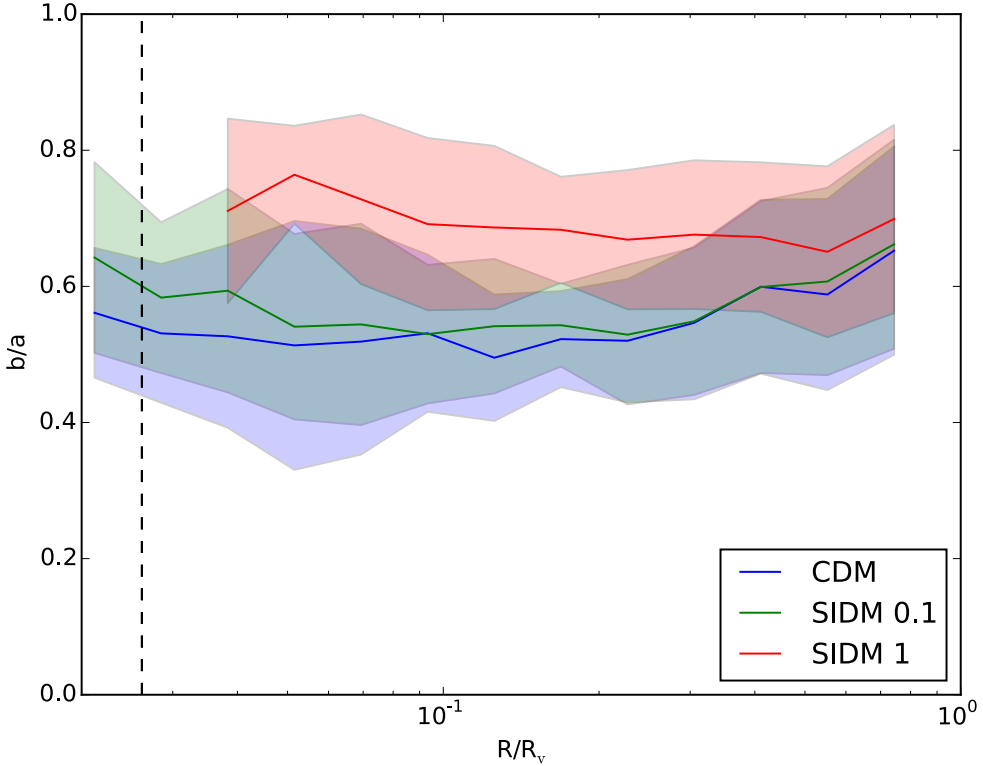


Figure 10: Similar to the  $c/a$  plot (see Figure 9), but instead showing the ratio of the intermediate to major axis ( $b/a$ ) vs the scaled radius ( $R/R_v$ ). Again we see a hint of a divergence between the SIDM 0.1 (green) and CDM (blue) distributions, but better statistics (more halos) are required to draw any sound conclusions. The difference between SIDM 1 and CDM is clear at most radii.

### 3.3 Assembly history

The mass assembly history was constructed by a code I created that traces each halo back from  $z=0$  through successive snapshots, picking the most likely progenitor based on mass proximity and on distance from the selected halo in the previous (lower redshift) snapshot.

Figure 11 shows the mass assembly history for all our 15 halos for the CDEM case. The clusters acquire mass through slow smooth accretion and a few merger events (clearly visible in the plot for some of the halos as sudden jumps in the curve).

The purpose of having the mass assembly histories for our halos is to try to understand the dispersion in the density profiles of halos of similar mass. At a fixed radius, it is well known that more massive halos are denser than less massive ones, while (at a fixed mass) more concentrated halos form earlier than less concentrated ones.

We use a simple measure for the “formation” time of a halo as the redshift where it acquires half of its mass today. This gives us a way to explore if the dispersion in the density profiles is related to when the halos assembled most of their mass.

Figure 12 is a first attempt to make this exploration, it shows the density at a fixed radius ( $4\epsilon$ ) as a function of  $V_{max}$  (a proxy of halo mass) for the different halos and cosmologies. The size of the symbols are proportional to the formation redshift, larger symbols corresponds to halos formed earlier. As expected for CDM, more massive halos (larger  $V_{max}$ ) are denser than less massive ones. This correlation is more or less preserved in the SIDM 0.1 case, while it disappears for SIDM 1 (see Figure 12 of Rocha et al. 2013 [41]). With the low number of halos we have, we detect no clear trend with formation redshift, but notice that the dispersion in SIDM 1 is smaller than in CDM.

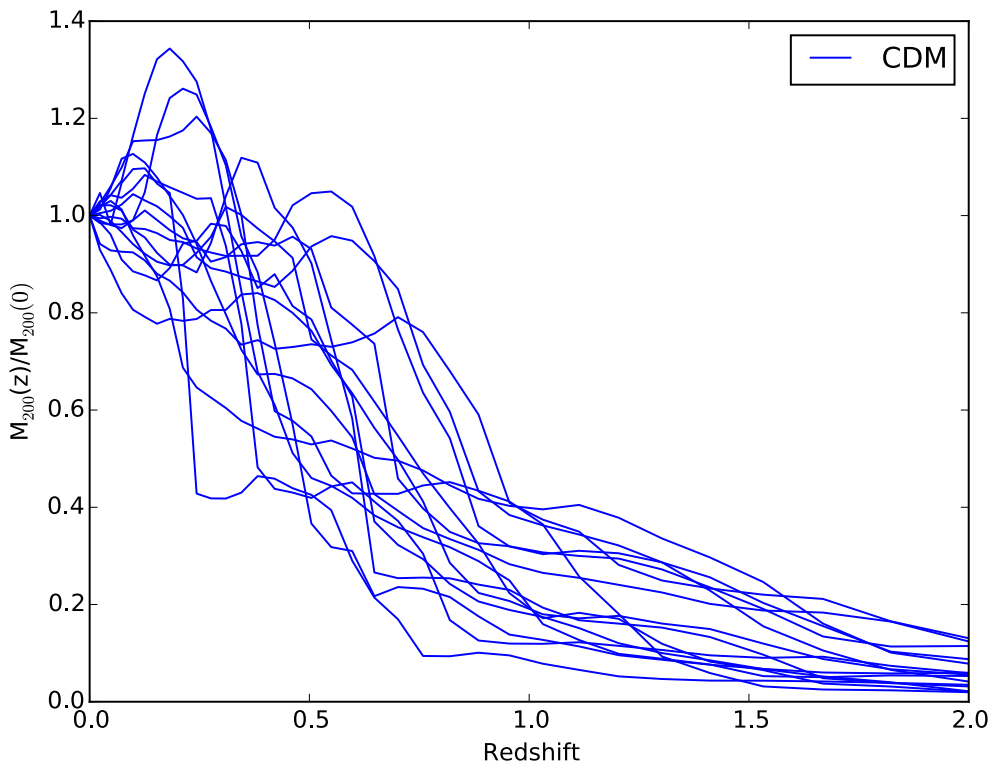


Figure 11: *Halo mass assembly history for our sample of halos: The virial mass as a function of redshift, scaled by  $M_{200}$  at  $z=0$ , vs redshift. We see halo growth by smooth accretion and some merger events indicated by large jumps in the mass of the system. The halo mass assembly history is almost identical for the SIDM halos, as SIDM does not in any significant way alter the virial mass of the halo.*

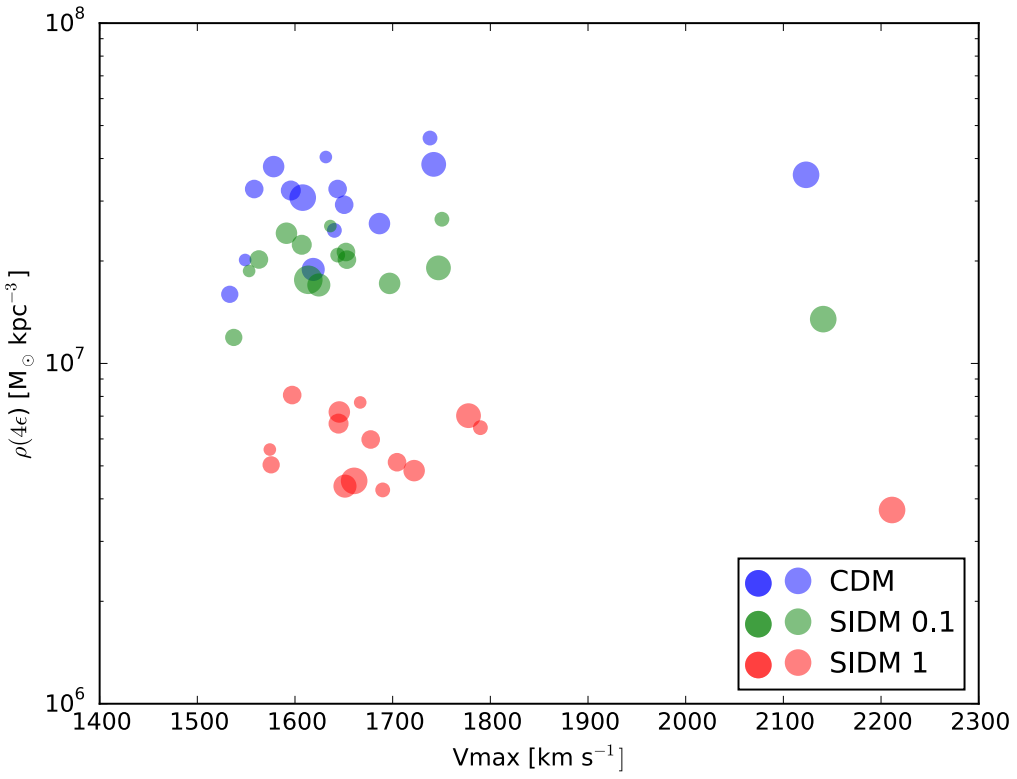


Figure 12: Density at four times the softening vs the maximum velocity of the halo (a proxy of halo mass). The type of simulation is shown by the color (blue for CDM, green for SIDM 0.1 and red for SIDM 1) and the symbol size indicates the square of the formation redshift (where the halo had obtained half its mass); meaning smaller symbols denote halos more recently formed whereas larger symbols indicate older halos. For the CDM (blue) and SIDM 0.1 (green) halos we see a mild correlation between the central density and the maximum velocity of a halo. We also see that SIDM 0.1 and SIDM 1 (red) have a slightly narrower distribution (lower dispersion) of around a factor of 2 compared to CDM which has around a factor of 3, indicating a smaller scatter in the central densities of SIDM halos.

## 4 Conclusion

I have performed high resolution N-body simulations of cluster-size dark matter halos within the Cold Dark Matter and Self-Interacting Dark Matter cosmologies. For the latter I used two values for a constant dark matter self-scattering cross section:  $0.1 \text{ cm}^2 \text{ gr}^{-1}$  (labeled SIDM 0.1) and  $1.0 \text{ cm}^2 \text{ gr}^{-1}$  (labeled SIDM 1). These values cover the interesting range where constant cross section SIDM is both allowed by observations and provides a solution to the structural problems of CDM at small scales.

After developing a set of analysis tools, more importantly a code to compute the principal axes of ellipsoidal shells centered in a halo, I have analyzed the structure of a sample of 15 cluster-size halos.

I have found that statistically I can differentiate SIDM halos from the CDM ones at the  $1\sigma$  level of a radius of  $\sim 15 \text{ kpc}$  ( $100 \text{ kpc}$ ) for a cross section per unit mass of  $0.1 \text{ cm}^2 \text{ gr}^{-1}$  ( $1.0 \text{ cm}^2 \text{ gr}^{-1}$ ). Given the impact of luminous matter in the inner dark matter distribution, I conclude that our DM-only simulations can potentially be used to constrain values close to  $1 \text{ cm}^2 \text{ gr}^{-1}$ , but likely not much lower.

The halo shapes, as given by the ratios of the principal axes, can also be used reliably to constrain the  $1.0 \text{ cm}^2 \text{ gr}^{-1}$  at even larger radii (a factor of a few) than in the case of the density profiles.

I performed a preliminary analysis of the dispersion of the distribution of density profiles and found that it is lower in SIDM than in CDM. In the latter there is a mild correlation with halo mass that disappears in SIDM 1. I also explored if the formation time of a halo (defined as the redshift where the halo acquired half of its mass today) plays any role in this dispersion, but found no clear trend.

For the future this work can be used to compare with the structure of observed galaxy clusters, by comparing the results obtained with the density profile and halo shapes obtained from X-Ray and Weak Lensing observations.

## References

- [1] Zwicky F., 1933, Helvetica Physica Acta **6**, 110-127
- [2] Babcock H. W., 1939, Lick Observatory Bulletin **19**, 41-51
- [3] Rubin V. C., Burstein D., Ford Jr. W. K., Thonnard N., ApJ **289**, 137-174
- [4] Fabricant D., Gorenstein P., 1983, ApJ **267**, 535-546
- [5] Markevitch M., Gonzalez A. H., David L., Vikhlinin A., Murray S., Forman W., Jones C., Tucker W., 2002, ApJ **567**, L27-31
- [6] Clowe D., Gonzalez A. H. & Markevitch M., 2004, ApJ **604**, 596-603
- [7] Milgrom M., 1983, ApJ **270**, 365-370
- [8] Bekenstein J. D., 2004, Phys. Rev. D. **70**, 8
- [9] Famaey B., McGaugh S. s., 2012, Living Rev. Relat. **15**, 10
- [10] Angus G. W., Famaey B., Buote D. A., 2008, MNRAS **387**, 1470-1480
- [11] Fan J., Katz A., Randall L., Reece M., 2013, Phys. Dark Univ **2**, 139
- [12] Gardner S., Fuller G. M., 2013, Prog. Part. Nucl. Phys. **71**, 167-184
- [13] Akerib D. S. et al., 2014, Phys. Rev. Lett. **112**
- [14] Springel V., 2005, MNRAS **364**, 1105-1134
- [15] Kuzio de Naray R., McGaugh S. S., de Blok W. J. G., 2008, ApJ **676**, 920-943
- [16] Walker M. G., Peñarrubia J., 2011, ApJ **742**, 20
- [17] Breddels M. A., Helmi A., 2013, A&A **558**, A35
- [18] Boylan-Kolchin M., Bullock J. S., Kaplinghat M., 2011, MNRAS **415**, L40-L44
- [19] Boylan-Kolchin M., Bullock J. S., Kaplinghat M., 2012, MNRAS **422**, 1203-1218
- [20] Pontzen A., Governato F., 2014, Nature **506**, 171-178
- [21] White S. D. M., Frenk C. S., Davis M., 1983, ApJ **274**, L1-L5
- [22] Abazajian et al., 2012, arXiv:1204.5379
- [23] Lovell M. R., Frenk C. S., Eke V. R., Jenkins A., Gao L., Theuns T., 2014, MNRAS **439**, 300-317
- [24] Spergel D. N., Steinhardt P. J., 2000, Phys. Rev. Lett. **84**, 3760
- [25] Zavala J., Vogelsberger M., Walker M. G., 2013, MNRAS **431**, L20-L24
- [26] Peter A. H. G., Rocha M., Bullock J. S., Kaplinghat M., 2013, MNRAS **430**, 105-120
- [27] Press W. H., Schechter P., 1974, ApJ **187**, 425-438
- [28] White S. D. M., 1976, MNRAS **177**, 717-733
- [29] White S. D. M., Rees M. J., 1978, MNRAS **183**, 341-358
- [30] Efstathiou G., Eastwood. J W., 1981, MNRAS **194**, 503-525
- [31] Centrella J., Melott A. L., 1983, Nature **305**, 196-198
- [32] Davis M., Huchra J., Latham D. W., Tonry J., 1982, ApJ **253**, 423-445
- [33] Davis M., Efstathiou G., Frenk C. S., White S. D. M., 1985, ApJ **292**, 371-394
- [34] Riess A. G. et al., 1998, Astronomy **116**, 1009-1038
- [35] Perlmutter S. et al., 1999, ApJ **517**, 565-586
- [36] Hanany S. et al., 2000, ApJ **545**, L5-L9

- [37] Springel V., White S. D. M., Jenkins A., Frenk C. S., Yoshida N. et al., 2008, *Nature* **435**, 629-636
- [38] Kuhlen, Vogelsberger & Angulo 2012
- [39] Oñorbe J., Garrison-Kimmel S., Maller A. H., Bullock J. S., Rocha M., Hahn O., 2014, *MNRAS* **437**, 1894-1908
- [40] Vogelsberger M., Zavala J., Loeb A., 2012, *MNRAs* **423**, 3740
- [41] Rocha M., Peter A. H. G., Bullock J. S., Kaplinghat M., Garrison-Kimmel S., Oñorbe J., Moustakas L. A., 2013, *MNRAS* **430**, 81-104
- [42] Ludlow A. D., Navarro J. F., Li M., Angulo R. E., Boylan-Kolchin M., Bett P., E., 2012, *MNRAS* **427**, 1322-1328
- [43] Power C., Navarro J. F., Jenkins A., Frenk C. S., White S. D. M., Springel V., Stadel J., Quinn T., 2003, *MNRAS* **338**, 14-34
- [44] Springel V., Wang J., Vogelsberger M., Ludlow A., Jenkins A., Helmi A., Navarro J. F., Frenk C. S., White S. D. M., 2008, *MNRAS* **391**, 1685-1711
- [45] Navarro J. F., Frenk C. S. & White S. D. M., 1997, *ApJ* **490**, 493-508
- [46] Hahn O., Abel T., 2011, *MNRAS* **415**, 2101-2121
- [47] Zemp M., Gnedin O. Y., Gnedin N. Y., Kravtsov A. V., 2011, *ApJS* **197**, 30
- [48] Zemp M., Moore B., Stadel J., Carollo C. M., Madau P., 2008, *MNRAS* **386**, 1543-1556